Supporting information

High-performance Asymmetric Electrode Structured Light-stimulated Synaptic Transistor for Artificial Neural Networks

Yixin Ran[#a], Wanlong Lu[#a], Xin Wang[#a], Zongze Qin[a], Xinsu Qin[b], Guanyu Lu [a], Zhen Hu [a], Yuanwei Zhu[a], Laju Bu[b], Guanghao Lu [*a].

[a.]Frontier Institute of Science and Technology, State Key Laboratory of Electrical Insulation and Power Equipment, Xi'an Jiaotong University, Xi'an，Shaanxi Province, 710054, China.

[b.] School of Chemistry, Xi'an Jiaotong University, Xi'an, Shaanxi Province, 710049, China.

[#.]These authors contribute equally.

(*The author to whom correspondence may be addressed: guanghao.lu@mail.xjtu.edu.cn)

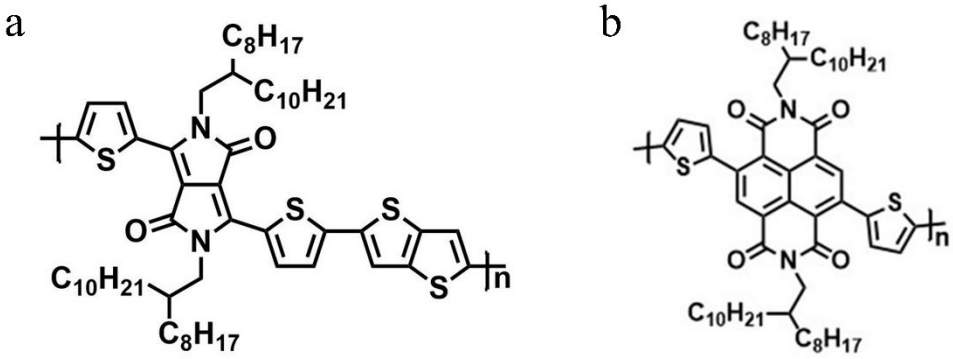

Figure S1. The respective molecular structures of DPP-DTT and N2200.

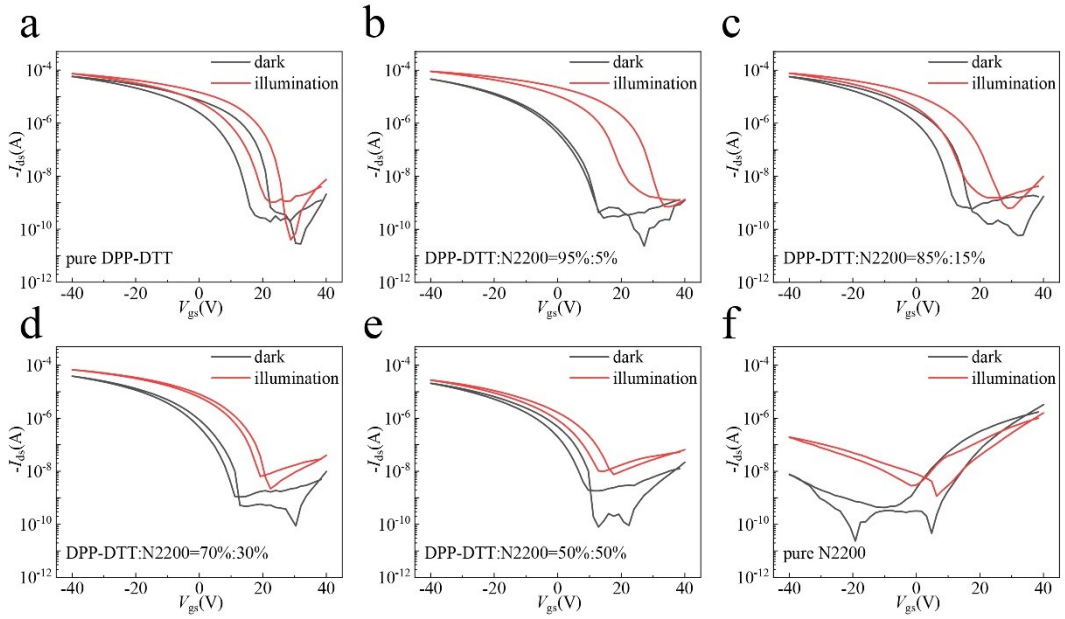

Figure S2. The transfer curves of different ratios of N2200 doped into DPP-DTT before and after experiencing light illumination.

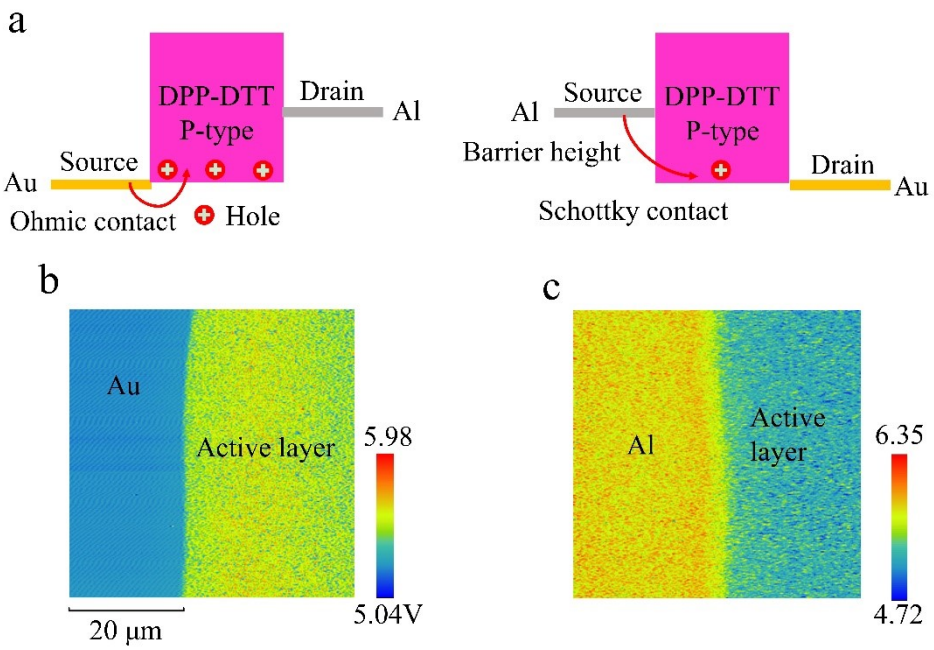

Figure S3. (a) Schematic diagram of the operating principle of the DPP-DTT: N2200 asymmetric electrode transistor device. Surface potential of asymmetric electrode devices. (b) Au acts as source electrode. (c) Al acts as source electrode.

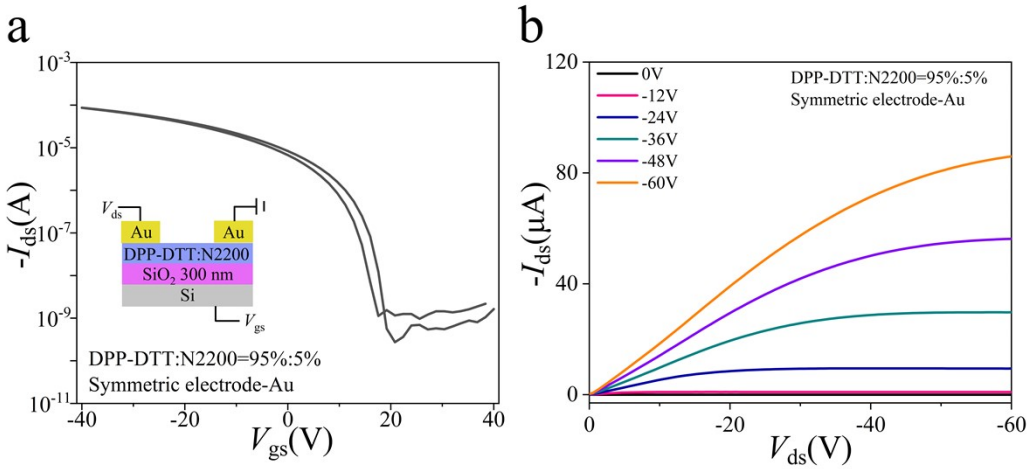

Figure S4. Transfer curve and output curve of conventional symmetrical electrode OFET. (a) Transfer curve. (b) Output curve.

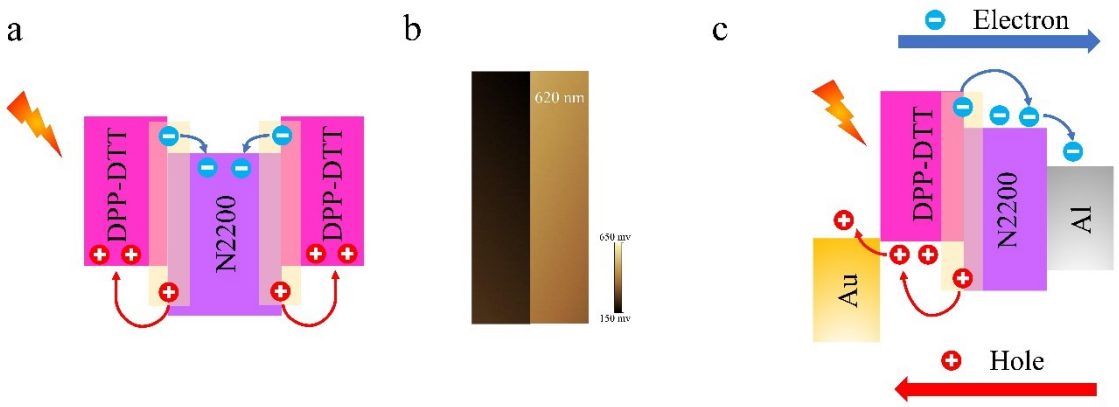

Figure S5. (a) Energy band during light illumination. (b) Surface potential of the blending film utilizing KPFM after light illumination. (c) Schematic diagram of asymmetric electrode device current becomes larger during light illumination.

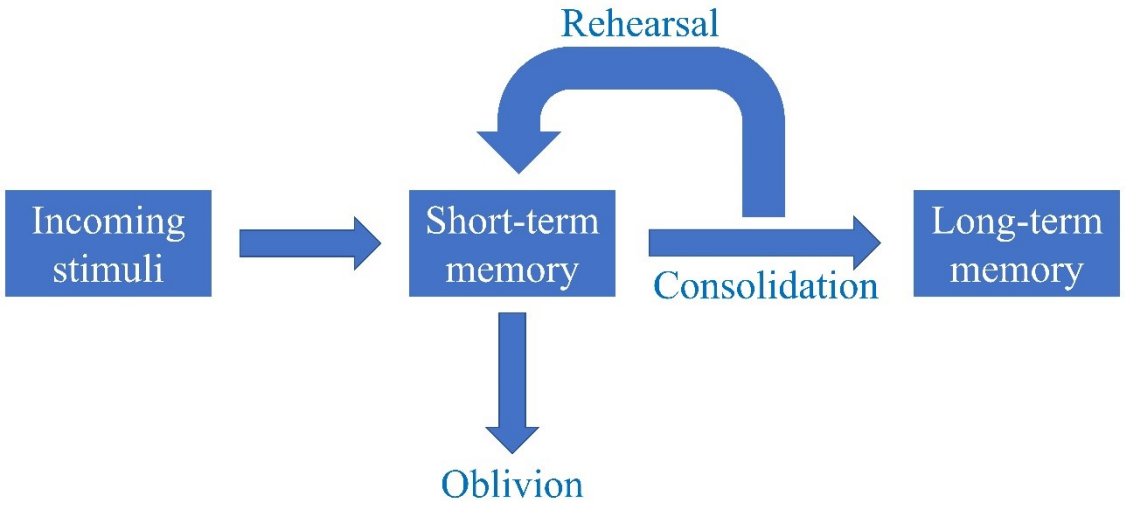

Figure S6. Schematic diagram of the human brain memory pattern.

Input		Output	
Light 1	Light 2	OR	AND
0	0	0	0
1	0	1	0
0	1	1	0
1	1	1	1

Figure S7. Truth table for the two logic functions of As-LSST.

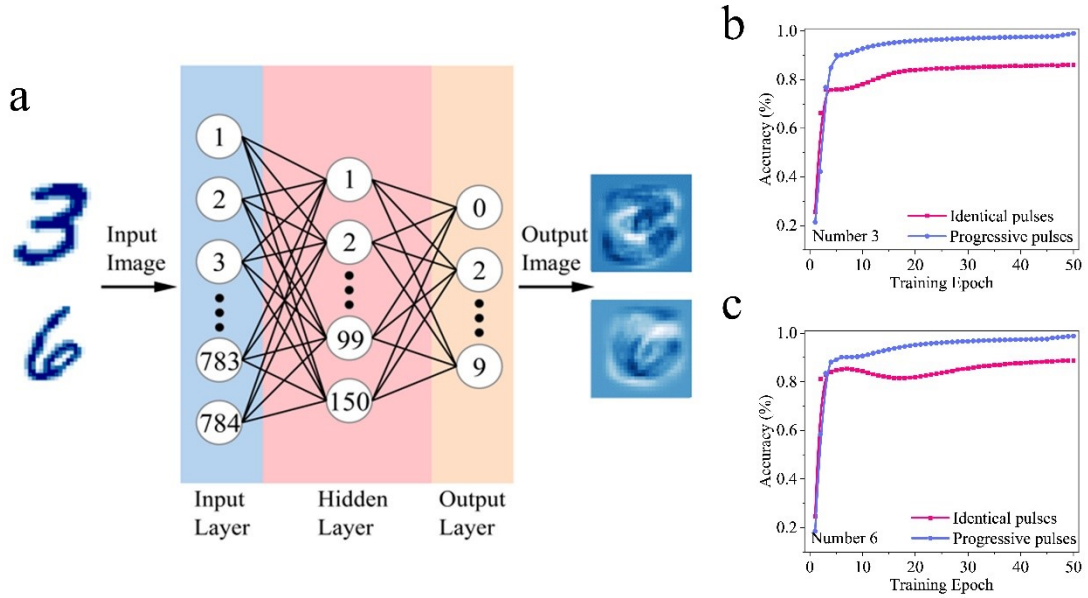

Figure S8. (a) Schematic diagram of the artificial neural network constructed by the As-LSST device used for the recognition task. Evolution of the recognition accuracy of the artificial neural network composed of As-LSSTs for handwritten digits: (b) number “3” and (c) number “6”.

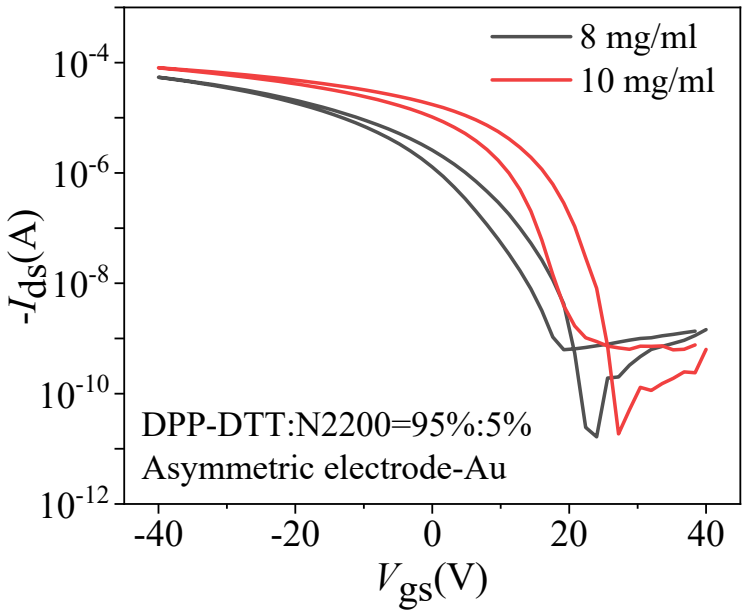

Figure S9. Transfer curves of asymmetric electrode devices for different semiconductor layer concentrations.

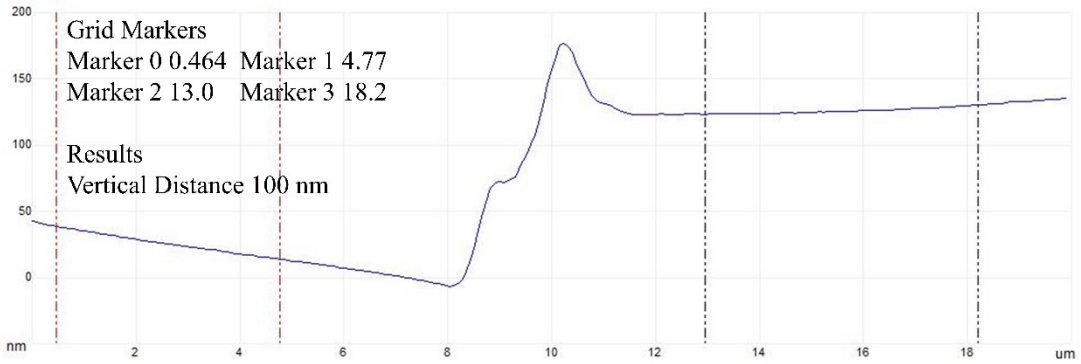

Figure S10. DPP-DTT: N2200 heterojunction film thickness.

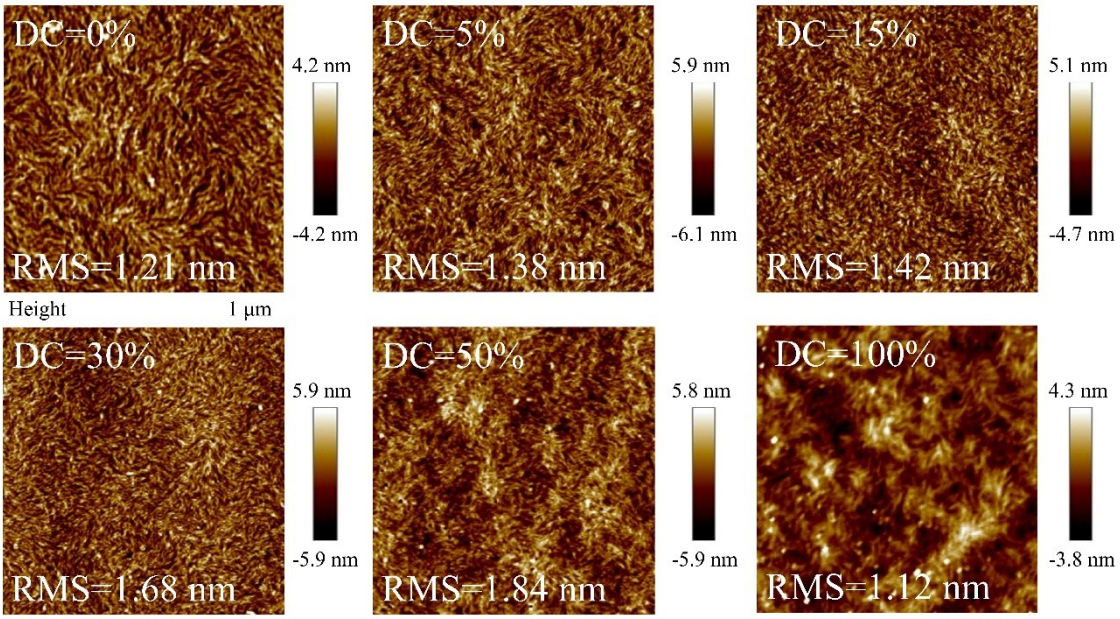

Figure S11. Topography images of thin films after doping with different ratios of N2200 into DPP-DTT.

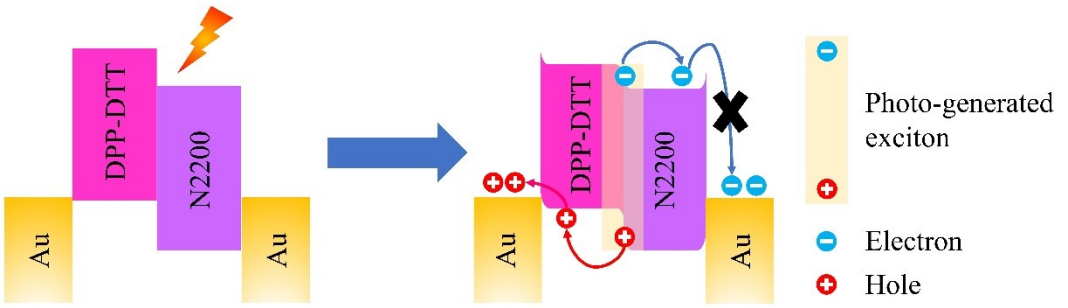

Figure S12. Schematic diagram of DPP-DTT: N2200 symmetric electrode device after illumination.

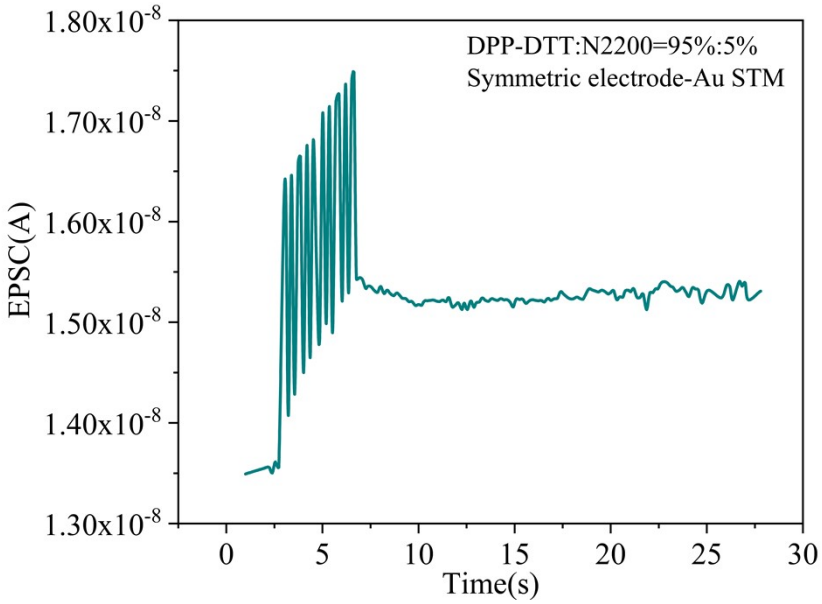

Figure S13. EPSC of DPP-DTT: N2200 symmetric electrode device after 10 light pulses of stimulation (V_g = 15 V, V_{ds} = -5 V).

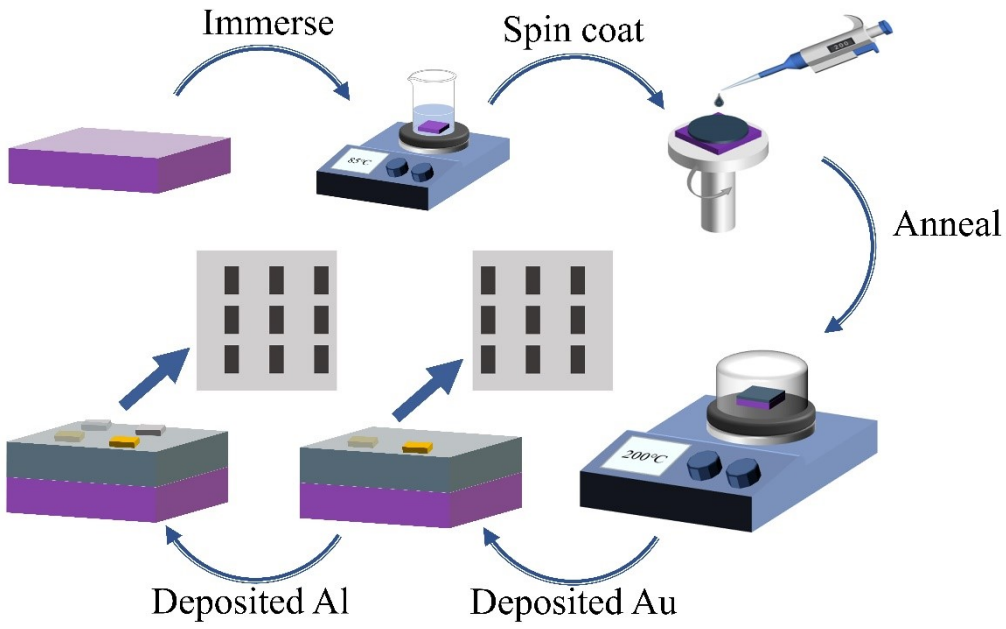

Figure S14. Schematic diagram of DPP-DTT: N2200 As-LSST device preparation.

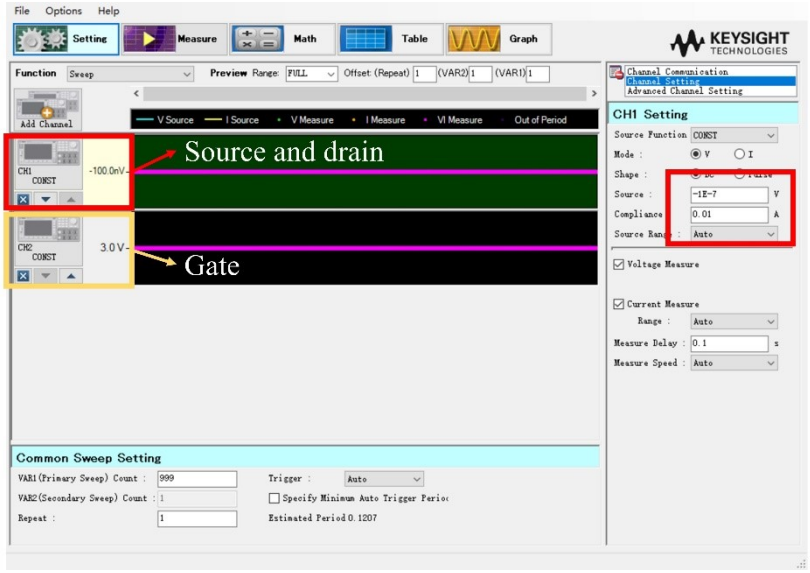

Figure S15. Parameter setting interface of an Agilent Keysight B2900A Quick IV measurement system.

Figure S16. Physical photography of an Agilent Keysight B2900A Quick IV measurement system.

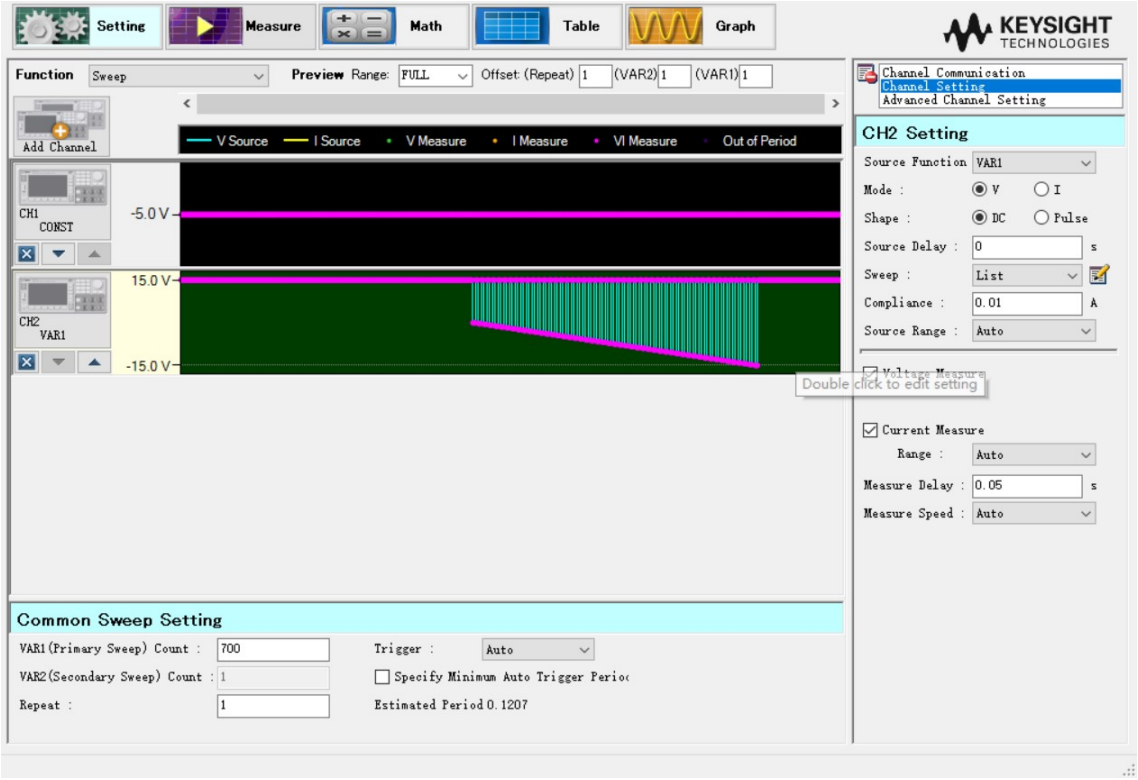

Figure S17. Digital recognition experiment condition setting interface by an Agilent Keysight B2900A Quick IV measurement system.